# The virtual node polygonal element method for nonlinear thermal analysis with application to hybrid laser welding

S.C. Wu[a,*], X. Peng[b], W.H. Zhang[a], S.P.A. Bordas[b]

[a]*State Key Laboratory of Traction Power,Southwest Jiaotong University, Chengdu 610031, China*

[b]*School of Engineering, Institute of Mechanics & Advanced Materials, Cardiff University, Queen's Building, the Parade, Cardiff, CF243AA, United Kingdom*

The nonlinear heat transfer process occurring during hybrid laser welding was simulated using the Virtual-node Polygonal Element (VPE) method within the framework of the Finite Element Method (FEM). To achieve robustness in large-scale welding simulations, a dynamic mesh refinement with quadtree and octree data structures was used in the welding region. Accuracy, convergence and efficiency were verified by solving two and three dimensional problems. It is found that the present VPE can successfully simulate the hybrid laser welding process with good accuracy and convergence. The adaptive refined mesh box can synchronously move with the welding heat source, which dramatically reduces the number of field nodes. Compared with the standard FEM,the VPEM requires only approximately 42% of the total degrees of freedom used in standard FEM for the same accuracy. Furthermore, we compare the computational cost and accuracy of the method to that of the finite element method, the edge based virtual node polygonal element/virtual node method, the edge-based Smoothed Point Interpolation Meshless Method (ES-PIM), the edge-based Element (ES-PIM), the Element Free Galerkin (EFG) method and the Meshless Local Petrove-Galerkin (MLPG) method. Compared to all those methods, the proposed scheme is found competitive in terms of computational cost versus accuracy, and benefit from a simple implementation.

*Keywords*: Polygonal element method; Hybrid laser welding; Transient heat transfer; Dynamic meshing refinement.

## 1. Introduction

Hybrid laser welding[1] has developed into a viable fusion joining method for aging hardened aluminum alloys because of its economic and technological advantages[2]. Nonetheless, the high heat sensitivity and low eutectic liquidus temperature range of certain alloys such as the Al-Zn-Mg-Cu series make it very difficult to produce a good-quality welded joint. To understand and control such complex metallurgical behaviors[3], it is necessary to accurately acquire the temperature field during and after

*Corresponding author. Tel.: +86-28-87634788, Fax: +86-28-87600868.
*E-mail address*: wusc@home.swjtu.edu.cn (S.C. Wu).

welding. The Finite Element Method (FEM)[4] is currently the most widely used numerical tool to predict the temperature history and resultant strain, stress and deformation for practical welding processes[5]. Unfortunately, the standard, well-developed FEM strongly depends on the elemental mesh, which may be inadequate for nonlinear thermomechanical analyses in the case of heat-induced distorted meshes[6].

To solve this problem, mesh-free methods have recently been developed that have allowed to avoid some of those difficulties. See Nguyen, 2008[7] for a review. Methods such as the Element-Free Galerkin (EFG) method[8], the Meshless Local Petrov-Galerkin (MPLG) method[9] and the Edge-based Smoothed Point Interpolation Method (ES-PIM)[10] have each specific advantages and drawbacks[7]. Despite the execllent accuracy and convergence rate as well as relative insensitivity to mesh quality, the excessive computational cost and the non-matural and disruptive implementation of mesh-free methods have limited their successful adoption in practical engineering applications[11]. This has motivated scientists and engineers to pursue numerical methods that are both closer in nature to the FEM but alleviate some of its shortcomings. For example, G R Liu developed the smoothed FEM, based on gradient smoothing, which yields a spectrum of methods with a spectrum of properties, depending on the number of sub-cells used for smoothing, their geometrical properties and distribution in the domain[12]. By constructing an independent “mesh” of sub-cells used to smooth the gradient, it is possible to obtain super-convergent, computationally cheap and accurate methods which are insensitive to mesh distortion and can be constructed for elements of arbitrary shape.

Another attempt is iso-geometric analysis (IGA) [13] which guarantees the preservation of the exact definition of the boundary of the domain during the CAD to Analysis transition. Such IGAFEM and IGABEM[14] enable to construct smooth approximations (a quality of most mesh-free methods) without sacrificing the ease of essential boundary condition enforcement characteristics of the FEM. IGA uses the rational functions for

the approximation, which, as in mesh-free methods, requires a “high” order quadrature, hence can make the method computationally expensive. Half quadrature rules were however designed for higher order approximation[15]. Enriched FEM, eg. PUFEM, GFEM, XFEM were also introduced to alleviate some of the difficulties associated with the FEM, in this case, the treatment of evolving discontinuities and singularities/boundary layers[16]. The XFEM and the SFEM were used conjointly in to rear benefits from both approaches [18].

In this paper, the Virtual-node Polygonal Element (VPE, or VNM, as it was originally called[19]) method is formulated to solve nonlinear heat transfer problems, in particular the welding thermal process due to a moving heat source for the first time. Combined with the quadtree (octree in 3D) mesh refinement strategy, mesh refinement follows the welding heat source to control the error and the computational cost. The VPE method is a partition of unity method [20] and is naturally suited to adaptive analyses by releasing the usual constraint on the element shape. Moreover, the VPE method is proposed within the classical FEM framework, and can be implemented easily within an existing finite element code.

## 2. VPE shape functions

The VPE method constructs the unknown temperature field by the least-squares method (LSM) coupled with an approximation of the constant strain elements (CSEs). Fig. 1 gives a typical polygonal domain $\Omega_k$ bounded by $\Gamma_k$ with $n$ scattered nodes: $\{p_1, p_2, \ldots, p_n\}$ and a centroid point $P_k$, in which $n$ is the total number of nodes in the polygon of interest.

The polygon can be divided into $n$ subtriangles $\{T_1, T_2, \ldots, T_n\}$. They are called virtual triangles because the vertex, *i.e.*, the geometric center $P_k$, is not associated with any degree of freedom (DOF). The temperature of $P_k$ can be evaluated by the least-squares method based on the $n$ nodes, which provides the nodal value for the shape function approximation in the CSEs.

Assuming the point of interest $p_I$ with the Cartesian coordinates $\mathbf{x}^{\mathrm{T}}=(x, y, z)$, the shape function of the VPE method can be defined as follows:

$$\Phi_I(\mathbf{x}) = w_i^{\mathrm{I}}(\mathbf{x})\left[\left(\delta_{iI}+\delta_{jI}\right)\varphi_I(\mathbf{x})+\varphi_k(\mathbf{x})\psi_I(\mathbf{x})\right]+w_i^{\mathrm{II}}(\mathbf{x})\psi_I(\mathbf{x}) \tag{1}$$

where the subscript $i$ of weight functions $w^{\mathrm{I}}$ and $w^{\mathrm{II}}$ representing the point of interest $p_I$ is located inside the $T_i$, $\varphi$ is the two-dimensional (2D) 3-node or three-dimensional (3D) 4-node approximation and $\psi$ is the least-squares approximation.

In Eq. (1), shape functions $\varphi$ and $\psi$ are constructed based on the area or volume coordinates of CSEs and the LSM [20], respectively:

$$\boldsymbol{\varphi}^{\mathrm{T}} = \left\{\varphi_i, \varphi_j, \varphi_k\right\} \tag{2}$$

$$\boldsymbol{\psi}^{\mathrm{T}} = \mathbf{p}^{\mathrm{T}}(\mathbf{x})\mathbf{A}^{-1}\mathbf{B} = \left\{\psi_1, \psi_2, \cdots, \psi_n\right\} \tag{3}$$

where ($\varphi_i$, $\varphi_j$, $\varphi_k$) are the shape functions obtained from the area or volume coordinates of node $I$ for an integration triangle, $\mathbf{p}$ is the complete polynomial basis built by the Pascal triangle, T is the matrix transpose operator, $\mathbf{A}=\Sigma\mathbf{p}(x_i)\mathbf{p}^{\mathrm{T}}(x_i)$ and $\mathbf{B}=[p(x_1), p(x_2),\ldots, p(x_n)]$, where $n$ is the total number of field nodes.

In addition, to provide interpolation properties, weight functions $w^{\mathrm{I}}$ and $w^{\mathrm{II}}$ are selected based on Eq. (2): $w^{\mathrm{I}}=\varphi_i+\varphi_j$ and $w^{\mathrm{II}}=\varphi_k$. This also ensures the important partition of unity property.

The unknown temperature field $\theta^h(\mathbf{x},t)$ is then approximated by

$$\theta^h(\mathbf{x},t) = \sum_{I=1}^{n}\Phi_I(\mathbf{x})\theta_I = \boldsymbol{\Phi}^{\mathrm{T}}(\mathbf{x})\boldsymbol{\theta}(\mathbf{x},t) \text{ in which } \boldsymbol{\theta} = (\theta_1, \theta_2, \cdots, \theta_n)^{\mathrm{T}} \tag{4}$$

Note that the derivatives can be obtained easily due to the polynomial form of the shape functions. It has been shown that the VPE approximation presents some good properties, such as continuity within the polygonal domain, $C^0$ continuity on the boundary of the arbitrary polygon $\Omega_k$, the Kronecker Delta property and linear completeness. These

attractive properties make the VPE method an efficient method for engineering problems.

## 3. Incremental discretized weak form

Consider a nonlinear transient thermal problem where material properties and boundary conditions are functions of the temperature and time. Assuming the domain is made up of a single material. The domain $\Omega$ is bounded by $\Gamma$ and the problem is to calculate the unknown temperature function $\theta(\mathbf{x}, t)$ that satisfies the following equations:

$$\mathrm{div}\,(k\cdot \mathrm{grad}\,\theta)+Q_w=\rho\cdot c\cdot\frac{\partial\theta}{\partial t} \qquad \text{for } \mathbf{x} \text{ in } \Omega,\ t>0 \qquad (5)$$

$$\theta=\theta_\Gamma \qquad \text{for } \mathbf{x} \text{ on } \Gamma_1,\ t>0 \qquad (6)$$

$$-(k\cdot \mathrm{grad}\,\theta)\cdot\mathbf{n}=-k\cdot\frac{\partial\theta}{\partial n}=q_\Gamma \qquad \text{for } \mathbf{x} \text{ on } \Gamma_2,\ t>0 \qquad (7)$$

$$-(k\cdot \mathrm{grad}\,\theta)\cdot\mathbf{n}=-k\cdot\frac{\partial\theta}{\partial n}=h_c\cdot(\theta-\theta_a) \qquad \text{for } \mathbf{x} \text{ on } \Gamma_3,\ t>0 \qquad (8)$$

$$-(k\cdot \mathrm{grad}\,\theta)\cdot\mathbf{n}=-k\cdot\frac{\partial\theta}{\partial n}=h_r\cdot(\theta-\theta_b) \qquad \text{for } \mathbf{x} \text{ on } \Gamma_4,\ t>0 \qquad (9)$$

$$-(k\cdot \mathrm{grad}\,\theta)\cdot\mathbf{n}=-k\cdot\frac{\partial\theta}{\partial n}=0 \qquad \text{for } \mathbf{x} \text{ on } \Gamma_5,\ t>0 \qquad (10)$$

$$\theta=\theta_{\mathrm{ini}} \qquad \text{for } \mathbf{x} \text{ in } \Omega,\ t=0 \qquad (11)$$

where $k_{\mathbf{x}}$ is the temperature-dependent heat conductivity, $\rho$ is the density, $c$ is the specific heat, $h_c$ is the convection coefficient and $h_r=\varepsilon\sigma(\theta^2+\theta_r^2)(\theta+\theta_r)$ is the surface radiation coefficient, in which $\varepsilon$ is the emissivity of a radiant surface, $\sigma$ is the Stefan-Boltzmann constant, $Q_w$ is the welding heat input, $\theta_\Gamma$ is the prescribed temperature, $q_\Gamma$ is the prescribed heat flux, $\mathbf{n}$ is the unit normal vector, $\theta_a$ is the ambient medium temperature, $\theta_r$ is the temperature of the outward radiating source, $\theta_b$ is the specified bulk temperature of the fluid medium and $\theta_{\mathrm{ini}}$ is the initial temperature.

Then, the variational formulation of the thermal differential equation of Eq. (5) and the boundary conditions of Eqs. (6)-(10) can be established as

$$\Pi = \int_{\Omega} \theta \rho c \frac{\partial \theta}{\partial t} \mathrm{d}\Omega + \int_{\Omega} \frac{1}{2} \left[ k_x \left( \frac{\partial \theta}{\partial x} \right)^2 + k_y \left( \frac{\partial \theta}{\partial y} \right)^2 + k_z \left( \frac{\partial \theta}{\partial z} \right)^2 \right] \mathrm{d}\Omega -$$

$$\int_{\Omega} \theta Q_v \mathrm{d}\Omega - \int_{\Gamma_2} \theta q_{\Gamma} \mathrm{d}\Gamma + \frac{1}{2} \int_{\Gamma_3} h_c (\theta - \theta_a)^2 \mathrm{d}\Gamma + \frac{1}{2} \int_{\Gamma_4} h_r (\theta - \theta_r)^2 \mathrm{d}\Gamma \qquad (12)$$

By invoking the stationarity of the above temperature field functional, the governing equations can be easily derived for the thermal system discretised by a set of arbitrary convex polygons. However, in a nonlinear transient heat transfer analysis, the incremental heat flow equilibrium[22] must also be satisfied. The temperature approximation at time $t+\Delta t$ can be written as

$$\int_{\Omega} \delta\theta^{t+\Delta t} \rho c \frac{\partial^{t+\Delta t} \theta}{\partial t} \mathrm{d}\Omega + \int_{\Omega} \delta \boldsymbol{\theta}^{\mathrm{T}\ t+\Delta t} \mathbf{k}^{\ t+\Delta t} \boldsymbol{\theta} \mathrm{d}\Omega = \int_{\Omega} \delta\theta^{t+\Delta t} Q_w \mathrm{d}\Omega + \int_{\Gamma_q} \delta\theta^{t+\Delta t} q_{\Gamma} \mathrm{d}\Gamma +$$

$$\int_{\Gamma_c} \delta\theta^{t+\Delta t} h_c \left( {}^{t+\Delta t}\theta - {}^{t+\Delta t}\theta_a \right) \mathrm{d}\Gamma + \int_{\Gamma_r} \delta\theta^{t+\Delta t} h_r \left( {}^{t+\Delta t}\theta - {}^{t+\Delta t}\theta_r \right) \mathrm{d}\Gamma \qquad (13)$$

where the conductivity matrix $\mathbf{k}$ is

$$\mathbf{k} = \begin{Bmatrix} k_x & 0 & 0 \\ 0 & k_y & 0 \\ 0 & 0 & k_z \end{Bmatrix} \text{ for 3D; } \mathbf{k} = \begin{Bmatrix} k_x & 0 \\ 0 & k_y \end{Bmatrix} \text{ for 2D} \qquad (14)$$

By using the backward Euler method, the full Newton-Raphson method and the shape functions of Eq. (1), we can obtain a temperature approximation for the hybrid laser process in the following set of algebraic equations at each iteration:

$${}^{t+\Delta t}\mathbf{K}^{(i-1)} \Delta\boldsymbol{\theta}^{(i)} = {}^{t+\Delta t}\mathbf{Q}_w + {}^{t+\Delta t}\mathbf{Q}_c^{(i-1)} + {}^{t+\Delta t}\mathbf{Q}_r^{(i-1)} - {}^{t+\Delta t}\mathbf{Q}_k^{(i-1)} \qquad (15)$$

The global stiffness and vectors[23] are then assembled based on these non-overlapping polygonal domains that are similar to elements used in FEM and can be solved using the Hammer integration[24], as illustrated in Fig. 1.

Note that the welding heat source is assembled in the global vector of $\mathbf{Q}_w$ and that the source energy distribution $[Q_t(\mathbf{x})=q_1(\mathbf{x})+q_2(\mathbf{x})]$ is simulated using the double ellipsoidal heat source model, as follows:

$$q_1(x,y,z)=\frac{6\sqrt{3}f_1Q_w}{abc_1\pi}\exp(-3\frac{x^2}{c_1^2})\exp(-3\frac{y^2}{a^2})\exp(-3\frac{z^2}{b^2}) \quad (16)$$

$$q_2(x,y,z)=\frac{6\sqrt{3}f_2Q_w}{abc_2\pi}\exp(-3\frac{x^2}{c_2^2})\exp(-3\frac{y^2}{a^2})\exp(-3\frac{z^2}{b^2}) \quad (17)$$

where $Q_w=\eta_1 UI+\eta_2 P$ is the total power of the electric arc and laser. In the simulation, we adopt the parameters $a$=0.004m, $b$=0.005m, $c_1$=0.0015m, $c_2$=0.003m, $U$=25V, $I$=110A, $P$=2.9kW, $\eta_1$=0.9, $\eta_2$=0.4, $f_1$=0.4, $f_2$=1.6.

## 4. Adaptive strategy

To ensure the numerical accuracy of the method, it is necessary to pregenerate a fine, regular mesh along the welding path, owing to the local steep temperature gradient. For large 3D engineering components, such a mesh would not be efficient, and adaptivity must be used to control the computational cost. The quadtree (octree) meshing strategy is an alternative to obtain a locally dense mesh and has been widely used in strong discontinuity problems of fracture mechanics [25]. Fig. 2 shows the hierarchical quadtree data structure at the element level refined for the 2D initial quadrilateral mesh. Due to the mismatch between adjacent elements, transition elements with hanging nodes on the element sides should be used; elements 2 and 3 are examples of this. The VPE method has proven to be a good choice to tackle these nonconforming elements since the 5-noded elements can be considered as pentagons and treated as usual, thereby requiring no special treatment.

By using the VPE method, an adaptive quadtree meshing strategy is deployed to dynamically refine and coarsen the mesh of a given domain that covers the moving welding heat source. This type of mesh refinement is performed independently for each incremental step in the thermal analysis.

Fig. 3 presents the detailed flowchart for 2D and 3D welding analyses using the proposed mesh refinement.

The mesh adaptation procedure can be further explained as follows:

**Step 1:** The elements to be refined are identified from the user-specified domain and then numbered as the latest added nodes in this refinement level. Note that the node index is counted from the total number of nodes in the previous level.

**Step 2:** Now the incremental initial nodal temperature for the latest added nodes should be given. If one latest added node appeared in the previous increment, its initial value is retrieved from the last incremental result. Once the node is added for the first time, the VPE interpolation in the original mesh is modified to retain its initial value.

**Step 3:** If *Nr* (*Nr* is the time of refinement) does not reach the maximum value, *Nr*←*Nr*+1 and return to Step 1. Otherwise, go to Step 4.

**Step 4:** Assemble the system equation for the final mesh and solve it to obtain the incremental solution for the nodal temperature.

**Step 5:** Save the overall latest added nodal values for the next iteration.

## 5. Numerical implementation

An intensive numerical study was performed to identify the accuracy, stability, convergence and efficiency of the VPE method for nonlinear transient thermal analyses. Linear and nonlinear transient heat transfer codes were developed using FORTRAN 6.6. Three norms of the relative temperature error, relative energy error and equivalent energy were used:

$$U_T = \int_\Omega \left(\partial\theta / \partial\mathbf{x}\right)^{\mathrm{T}} \mathbf{k} \left(\partial\theta / \partial\mathbf{x}\right) \mathrm{d}\Omega \tag{18}$$

$$R_T = \sqrt{\frac{\int_\Omega \left(\theta_{ref} - \theta_{\mathrm{VPE}}\right)^2 \mathrm{d}\Omega}{\int_\Omega \theta_{ref}^2 \mathrm{d}\Omega}} \tag{19}$$

$$R_E = \sqrt{\frac{\int_\Omega \left(\partial\boldsymbol{\theta}_{ref}/\partial\mathbf{x} - \partial\boldsymbol{\theta}_{\mathrm{VPE}}/\partial\mathbf{x}\right)^{\mathrm{T}} \boldsymbol{k} \left(\partial\boldsymbol{\theta}_{ref}/\partial\mathbf{x} - \partial\boldsymbol{\theta}_{\mathrm{VPE}}/\partial\mathbf{x}\right) \mathrm{d}\Omega}{\int_\Omega \left(\partial\boldsymbol{\theta}_{ref}/\partial\mathbf{x}\right)^{\mathrm{T}} \mathbf{k} \left(\partial\boldsymbol{\theta}_{ref}/\partial\mathbf{x}\right) \mathrm{d}\Omega}} \tag{20}$$

where the subscript *ref* denotes the exact or reference solution obtained from the relevant numerical method using a very fine mesh and $T$ and $E$ were the temperature norm and energy norm, respectively.

### 5.1 Patch test

For a numerical method to be suitable for energy transformation systems, it is sufficient for the method to pass the standard patch test. To investigate the accuracy and convergence of the VPE method, Fig. 4 gives four cases of arbitrary elemental meshes for the CSE (Case A uses a triangular mesh and B, a quadrilateral mesh), the nonconforming quadtree mesh (Case C uses a quadtree mesh) and the VPE mesh (Case D uses a convex polygon).

Both the left and right sides of the rectangular domain were prescribed to be adiabatic boundaries, and a constant temperature was prescribed on the remaining two sides by $\theta_\Gamma=\theta$. Satisfaction of the linear patch test then requires that the temperature of any interior nodes be given by the same linear function and that the temperature gradients be constant. Thus, the exact nodal temperature can be computed according to the longitudinal coordinate.

For the FEM patch tests, one Hammer integration point was used in the linear 3-noded CSE of Case A, and 2×2 Gaussian integration points were used in the bilinear 4-noded quadrilateral element of Case B. For the VPE patch tests, only one Hammer integration point was adopted in the virtual subtriangle. Table 1 gives the error comparisons of the relative temperature and energy.

It can be clearly observed that the relative temperature and energy accuracies of the VPE method are very stable, with a magnitude of $10^{-13}$ , near the machine precision, and

that the same precision as the standard FEM is retained, regardless of the element type and size. Moreover, the VPE method can provide good precision, even though extremely irregular polygonal elements or quadtree elements were used. In contrast, conventional polygonal finite elements formulated using the Wachspress, Mean-value and Laplace methods cannot achieve a similar precision, even though more nodes and a finer mesh are used[26].

Based on the above comparisons, it is confirmed that the present VPE method can pass the patch test with higher accuracy. The results also indicate that the VPE method is superior to conventional FEM and polygonal finite element methods.

### 5.2 Linear heat transfer with mixed boundary conditions

To further investigate the VPE formulation, a 2D linear model with mixed thermal boundary conditions is illustrated in Fig. 5. The material properties are defined as follows: $\rho$=7823 kg/m$^3$, $k_x$=$k_y$=52 W/m $^o$C, $c$=434 J/kg $^o$C.

Four cases of irregular quadrilateral meshes with 149, 530, 826 and 1241 nodes are designed to examine the convergence and accuracy. A reference solution with 12000 nodes is also provided using ABAQUS. The numerical equivalent energies have been plotted against the number of nodes in Fig. 6. The temperature distribution along edge CD is plotted in Fig. 7 for FEM, the VPE method and the reference.

It can be observed that both the VPE method and the standard FEM possess the lower-bound property at an equivalent energy, *i.e.*, their equivalent energies are always lower than the exact energy. Both implementations converge to the reference solution. Moreover, the VPE method is more accurate than the conventional FEM. From Fig. 7, it is observed that the temperature computed with the VPE method is in good agreement with the reference and FEM solutions, which verifies the implementation of the VPE method.

### 5.3 Moving heat source

Welding involves rapid heating and cooling. To investigate the robustness of the local meshing adaptation proposed in Section 4, Fig. 8 provides a 2D nonlinear computational model.

The hybrid laser welding heat source is simulated by a bi-ellipse distributed body heat flux. In this implementation, a user-defined Subroutine Dflux is developed into the ABAQUS interface to model the moving heat source defined in Eqs. (16) and (17). The welding travel speed is 40 mm/s. To model the welding moving heat source, the ABAQUS-based subroutine Dflux is developed, which provides the FEM reference solution for the VPE method. Age-hardened 7075-T6 aluminum alloy is used, and the thermal physical properties are plotted in Fig. 9.

Highly concentrated welding energy leads to a sharp temperature and strain gradient in the vicinity of melted metals. To achieve the accuracy, very fine regular meshes are often needed near the welded zone, while other zones use coarse mesh. This arrangement might produce distorted transition elements, especially when using triangular and tetrahedral elements. The existence of transition elements may degrade the precision of the solution. Fig. 10 gives the grade-distributed mesh with 1200 quadrilateral elements.

Fig. 11 shows the temperature curves of sample points $P_1$, $P_2$, $P_3$ and $P_4$, calculated using both the VPE method and the FEM. Note that the material nonlinearity due to the temperature variation is excluded in the present computation, and the corresponding properties used can be interpolated at 20°C from Fig. 10.

It is obviously observed that the VPE method achieves accuracy comparable to that obtained from FEM. This shows that the VPE method can be considered an alternative method to conventional FEM for thermal problems.

In practical cases, material properties change because of the thermal cycle, which notably affects the microstructures and mechanical performance of welded joints. It is

therefore necessary to consider temperature-dependent physical properties. Fig. 12 shows a coarse mesh in which the elemental size is twice as large within the region ABEF than that plotted in Fig. 10 and ECDF has a somewhat coarser mesh.

The quadtree mesh is then introduced based on the meshing scheme in section 4. The rectangular mesh box has the same elemental density as that of region ABEF, as shown in Fig. 10. Thus, the mesh box can synchronously travel with the welding heat source, which successfully allows for the dynamic addition and removal of elements. Fig. 13 is a plot of the quadtree adaptive mesh refinement and coarsening with a moving mesh box, which simulates the welding heat source. The temperature evolution at four sample points are calculated using the VPE method for the comparison with results obtained using the fine mesh in Fig. 10 using the standard FEM.

Fig. 14 shows the temperature at sample points $P_1$, $P_2$, $P_3$ and $P_4$, respectively. The figure compares the effect of different welding thermal cycles. The VPE method is implemented within a robust code using the quadtree mesh adaptation, while the FEM results are provided by ABAQUS.

It can be observed that both methods yield almost identical temperature evolutions. More importantly, the number of additional elements in Fig. 13 using the VPE method is insignificant compared with those in Fig. 10 for standard FEM. Fig. 15 clearly illustrates the analysis states of an adaptive refined mesh (total 581 nodes) at 0.5 s, 2.5 s and 4.9 s.

According to results from both Fig. 14 and Fig. 15, the adaptive VPE method can provide accuracy comparable to that of standard FEM without adaptation, even though only approximately 41% of DOFs are used.

### 5.4 Hybrid welding in 3D

All engineering structures and components are complicated in terms of spatial geometry, and the 2D models are usually insufficient to realistic physical system. For 3D problems, a convex polytope is divided into subtetrahedral domains for the Hammer integration.

The 2D model can be easily extended into the spatial case with a thickness of 6 mm. In this 3D examination, a butt welding joint with a size of $100\times48\times6$ mm$^3$ is first created using standard FEM for two meshes. The material used is a 7075-T6 alloy with physical properties given in Fig. 9, and the welding speed is taken as 40 mm/s. The butt surface of two of the plates has adiabatic boundary conditions, and the other plates are assigned convection boundary conditions.

Fig. 17 provide comparisons of the nonlinear transient temperature field using standard FEM based on a coarse and a fine mesh, respectively.

It can be concluded from the above comparisons that the finer mesh produces a lower peak temperature. For the refined mesh in Fig. 17, the total CPU time is approximately 42.5 hours under the same solver and hardware conditions used previously.

To increase the computational efficiency (CPU time for the same accuracy in energy norm), the refined mesh is only required under the welding torch. The size of the refined mesh "box" along the $x$, $y$ and $z$ axis is $d*s^{r-1}$, $0.5*d*s^{r-1}$ and $0.5*d*s^{r-1}$, respectively, where $d$=0.022 and scale coefficient $s$=0.6, $r$ is the times of refinement. The proposed mesh refinement strategy is thus introduced. Fig. 18 gives the temperature field at $t$=1.25 s with one refinement based on the coarse mesh used in Fig. 16. Fig. 19 gives the temperature field with two refinements based on the above refined mesh.

Note that the total time of $t$=1.25 s in the foregoing figure captions indicates the real welding time rather than the CPU time. It can be clearly a single refinement provides the same accuracy with only 2.5 times the number of nodes at initial (level 0) mesh, whilst the standard FEM requires approximately 5.8 times the original number of nodes. Moreover, the total CPU time is approximately 21.5 hours, which is about half of the total computational cost for the FE mesh of Fig. 17.

In addition, the VPE method is also distinctly superior to well-developed mesh-free methods. For the same elemental mesh in Fig. 18, EFG, MLPG and ES-PIM[27] require approximately 96 hours, 145 hours and 62 hours, respectively. In contrast, the present

VPE method demonstrates a significant advantage in this area, especially for large-scale engineering analyses.

## 6. Conclusions

The proposed VPE method has been formulated to model 3D nonlinear transient heat transfer phenomena during the hybrid laser welding process. The validity and robustness are examined in terms of numerical accuracy, convergence and efficiency. To solve this type of highly concentrated thermal problem, such as that caused by hybrid laser welding, the dynamic meshing refinement strategy is developed and applied to simulating the heat transfer process during and after welding. Both 2D and 3D welding cases are carried out, and conclusions can be made as:

(1) The proposed VPE method can successfully solve the nonlinear thermal response to the welding process with better accuracy compared with FEM. To achieve a similar solution accuracy, only approximately 42% of the total DOFs in standard FEM are used by the present VPE method. Among well-developed numerical methods, the computational cost in the frame work of FEM can be ranked in the ascending order VPE→FEM→ ES-PIM→EFG→MLPG under the same elemental mesh.

(2) The dynamic refined meshing box is adopted to locally refine the mesh in the vicinity of the heat source. The refining times and the size of the adaptive meshing can be adjusted freely, to obtain a best compromise between the model size and precision.

Future works may go on the realization of mechanical-thermal coupled model for welding process using the dynamic mesh box in the context of VPE method. The enrichment idea based on the partition of unity theory [20] is also a good alternative to capture the high gradient field while decreasing the mesh density.

## Acknowledgements

Financial support is mainly provided by the National Nature Science Foundation of China (Grant No.: 51005068), the Fundamental Research Funds for the Central University (Grant No.: 2682013CX030), the Self-developed Research Project of the State Key Lab of Traction Power (2013TPL_T18) and the China Postdoctoral Science Foundation (Grant No.: 2013M531980). Thanks are given for the partial support from the Open Research Fund Program of the State Key Lab of Advanced Design and Manufacturing for Vehicle Body (Grant No.: 31115030) and the Open Research Fund Program of the State Key Lab of Traction Power (TPL1302).

## References

[1] H. Staufer. Laser hybrid welding in the automotive industry. Welding Journal, 2007, 86(10): 36~40.

[2] W. Piekarska, M. Kubiak. Three-dimensional model for numerical analysis of thermal phenomena in laser-arc hybrid welding process. International Journal of Heat and Mass Transfer, 2011, 54(23-24): 4966~4974.

[3] B. Hu, I.M. Richardson. Microstructure and mechanical properties of AA7075 (T6) hybrid laser/GMA welds. Materials Science and Engineering A, 2007, 459(1-2): 94-100.

[4] R.W. Lewis, K. Morgan, H.R. Thomas, K.N. Seetharamu. The Finite Element Method in Heat Transfer Analysis. John Wiley & Sons, New York, 1996.

[5] A. Anca, A. Cardona, J. Risso, V.D. Rachinotti. Finite element modeling of welding processes. Applied Mathematical Modelling, 2011, 35(2): 688~707.

[6] O.C. Zienkiewicz, R.L. Taylor. The Finite Element Method. Butterworth-Heinemann, Oxford, 2002.

[7] V. P. Nguyen, T. Rabczuk, S. Bordas, M. Duflot. Meshless methods: A review and computer implementation aspects. Mathematics and Computers in Simulation, 79(3), 763–813.

[8] I.V. Singh. Meshless EFG method in three-dimensional heat transfer problems: a numerical comparison, cost and error analysis. Numerical Heat Transfer A, 2004, 46(2): 199~220.

[9] M. Shibahara, S.N. Atluri. The meshless local Petrov-Galerkin method for the analysis of heat conduction due to a moving heat source in welding. International Journal of Thermal Sciences, 2011, 50(6): 984~992.

[10] S.C. Wu, G.R. Liu, X.Y. Cui, T.T. Nguyen, G.Y. Zhang. An edge-based smoothed point interpolation method (ES-PIM) for heat transfer analysis of rapid manufacturing system.

International Journal of Heat and Mass Transfer, 2010, 53(11-12): 1938~1950.

[11] L.E. Lindgren. Finite element modeling and simulation of welding, Part 3: Efficiency and Integration. Journal of Thermal Stresses, 2001, 24(4): 305~334.

[12] G. R. Liu. A generalized gradient smoothing technique and the smoothed bilinear form for Galerkin formulation of a wide class of computational methods. International Journal of Computational Methods, 05(02), 199–236.

[13] T. Hughes, J. Cottrell, Y. Bazilevs. Isogeometric analysis: CAD, finite elements, NURBS, exact geometry and mesh refinement, Computer Methods in Applied Mechanics and Engineering, 2005, 194 (39-41), 4135–4195.

[14] R. N. Simpson, S. Bordas, J. Trevelyan, T. Rabczuk. A two-dimensional Isogeometric Boundary Element Method for elastostatic analysis. Computer Methods in Applied Mechanics and Engineering, 2012, 209–212(0), 87–100.

[15] T. Hughes, A. Reali, G. Sangalli. Efficient quadrature for NURBS-based isogeometric analysis. Computer Methods in Applied Mechanics and Engineering, 2010, 199(5-8), 301–313.

[16] S. Bordas, S. Natarajan. On the performance of strain smoothing for quadratic and enriched finite element approximations (XFEM/GFEM/PUFEM). International Journal for Numerical Methods in Engineering, 2011, 86(4-5), 637–666.

[17] S. Natarajan, S. Bordas, D.R. Mahapatra. Numerical integration over arbitrary polygonal domains based on Schwarz-Christoffel conformal mapping. International Journal for Numerical Methods in Engineering, 2009, 80(1), 103–134.

[18] L. Chen, T. Rabczuk, S. Bordas, G. R. Liu, K. Y. Zeng, P. Kerfriden. Extended finite element method with edge-based strain smoothing (ESm-XFEM) for linear elastic crack growth. Computer Methods in Applied Mechanics and Engineering, 2012, 209-212, 250–265.

[19] X.H. Tang, S.C. Wu, C. Zheng, J.H. Zhang. A novel virtual node method for polygonal elements. Applied Mathematics and Mechanics-English Edition, 2009, 30(10): 1233-1246.

[20] J. M. Melenk, I. Babuška. The partition of unity finite element method: Basic theory and applications. Computer Methods in Applied Mechanics and Engineering, 1996, 139(1-4), 289–314.

[21] N. Sukumar, E.A. Malsch. Recent advances in the construction of polygonal finite element interpolants. Archives of Computational Methods in Engineering. 2006, 13(1): 129~163.

[22] K.J. Bathe, M.R. Khoshgoftaar. Finite element formulation and solution of nonlinear heat transfer. Nuclear Engineering and Design, 1979, 51(2): 389~401.

[23] Z.B. Zhang, S.C. Wu, G.R. Liu, W.L. Chen. Nonlinear transient heat transfer problems using the meshfree ES-PIM. International Journal of Nonlinear Sciences & Numerical Simulation, 2010, 11(12): 1077~1091.

[24] P.C. Hammer, O.P. Marlowe, A.H. Stroud. Numerical integration over symplexes and cones. Math. Tables Aids Comp., 10:130-137,1956.

[25] A. Tabarraei, N. Sukumar. Extended finite element method on polygonal and quadtree meshes. Computer Methods in Applied Mechanics and Engineering, 2008, 197(5): 425~438.

[26] N. Sukumar, A. Tabarraei. Conforming polygonal finite elements. International Journal for Numerical Methods in Engineering, 2004, 61(12): 2045-2066.

[27] G.R. Liu, Y.T. Gu. An Introduction to Meshfree Methods and Their Programming. Springer Press, Netherlands, 2005.

## Table Captions

Table 1. Relative errors for all mesh cases

| Mesh cases | | A | B | C | D |
|---|---|---|---|---|---|
| $R_T$ | FEM | 2.14154494E-13 | 1.63559605E-13 | —— | —— |
| | VPE | 2.14219501E-13 | 1.64040944E-13 | 1.99594365E-13 | 1.56392254E-13 |
| $R_E$ | FEM | 4.70036018E-13 | 3.00659561E-13 | —— | —— |
| | VPE | 4.70515745E-13 | 2.99271054E-13 | 3.72428510E-13 | 3.78466797E-13 |

## Figure Captions

Fig. 1. Illustration of constructing interpolation and integration domains by dividing $\Omega_k$ into subtriangles with virtual points $P_k$.

Fig. 2. The element is divided into subelements by the quadtree rule.

Fig. 3. Flowchart for the refined mesh system in one incremental step.

Fig. 4. Mesh used in the VPE method for the patch test.

Fig. 5. Linear heat transfer model with dimensions and boundary conditions.

Fig. 6. Comparisons of the equivalent energy obtained using the present VPE method and FEM based on the same elemental mesh, together with the FEM reference result.

Fig. 7. Temperature distribution along edge CD with 530 nodes.

Fig. 8. Schematic model of plate butt welding with detailed dimensions, sampled points and boundary conditions.

Fig. 9. Material thermal properties in the hybrid welding simulation.

Fig. 10. Case 1: Fine mesh for the VPE method and FEM with 1414 nodes.

Fig. 11. Temperature history at reference points $P_1$, $P_2$, $P_3$ and $P_4$.

Fig. 12. Coarse mesh (408 nodes and 350 elements) with a larger elemental size.

Fig. 13. Case 2: quadtree meshing refinement based on the coarse mesh.

Fig. 14. Temperature history at the reference points in cases 1 and 2.

Fig. 15. Temperature fields and meshing states simulated using the present VPE method with dynamic meshing adding and subtracting technology at 0.5 s, 1.5 s and 4.9 s.

Fig. 16. Temperature distribution at $t$=1.25 s based on the coarse mesh (2448 nodes, 1650 elements) using standard FEM.

Fig. 17. Temperature distribution at $t$=1.25 s based on the fine mesh (14140 nodes, 11400 elements) using standard FEM.

Fig. 18. Temperature distribution at $t$=1.25 s based on the coarse mesh (2448+3606 nodes, 1650+2898 elements) with one refinement using the present VPE method.

Fig. 19. Temperature distribution at $t$=1.25 s based on the coarse mesh (6054+9491 nodes, 4548+8233 elements) with two refinements using the present VPE method.

**Figure 1.**

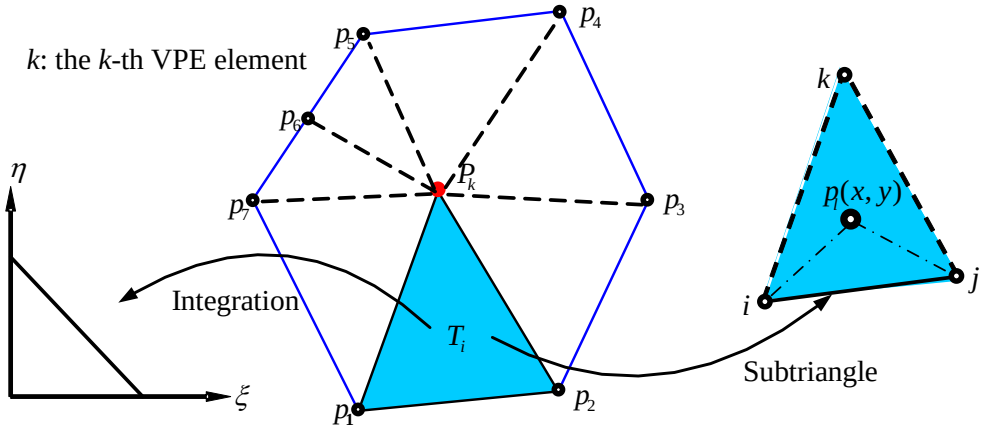


**Figure 2.**

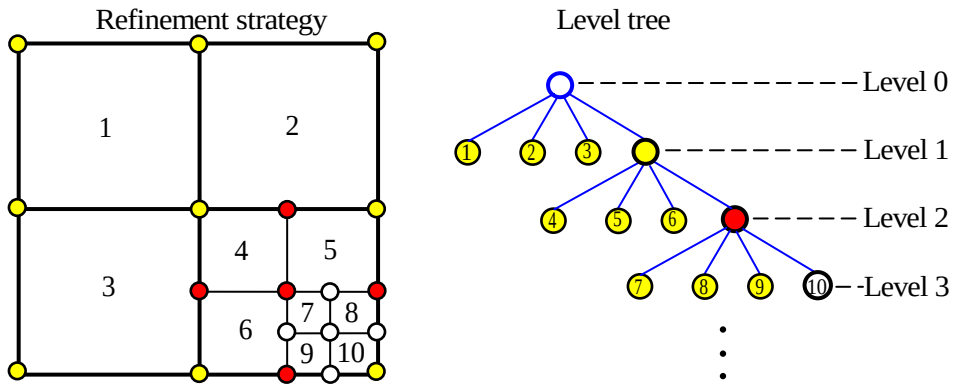

**Figure 3.**

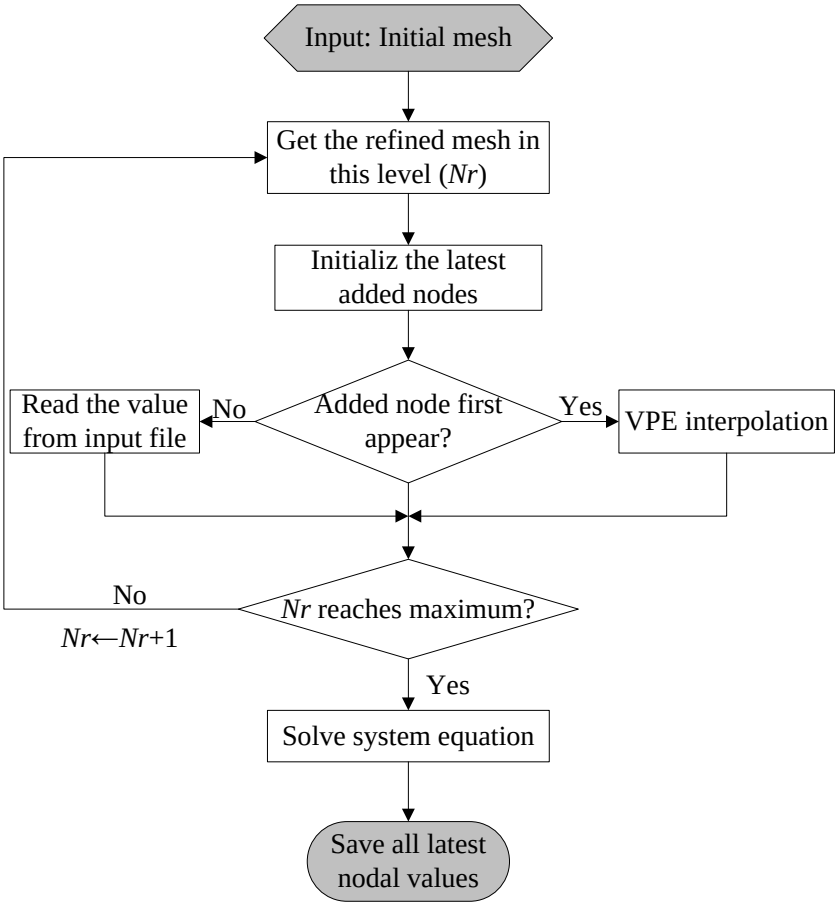


**Figure 4.**

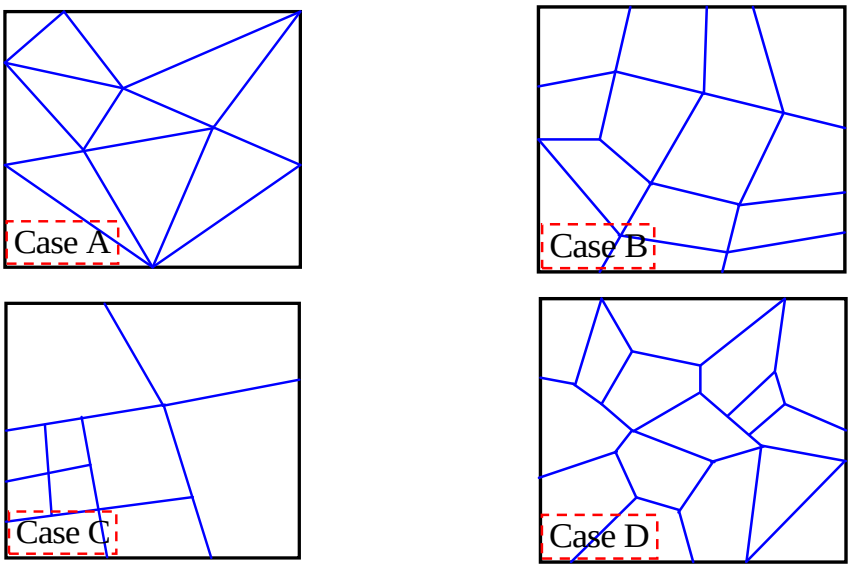

**Figure 5.**

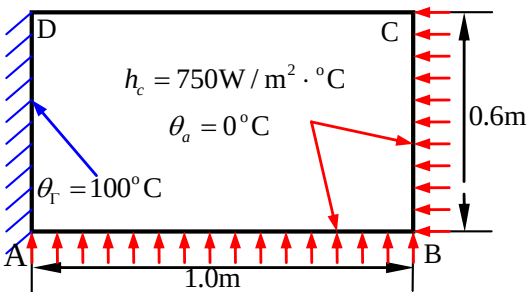


**Figure 6.**

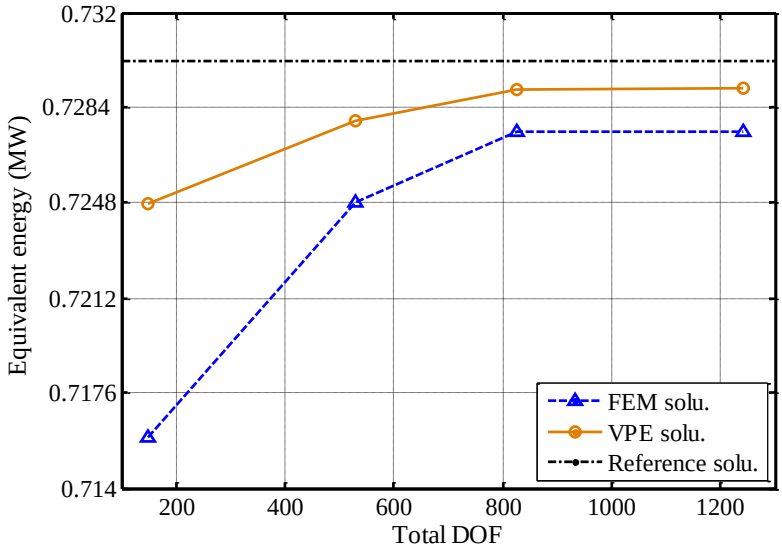


**Figure 7.**

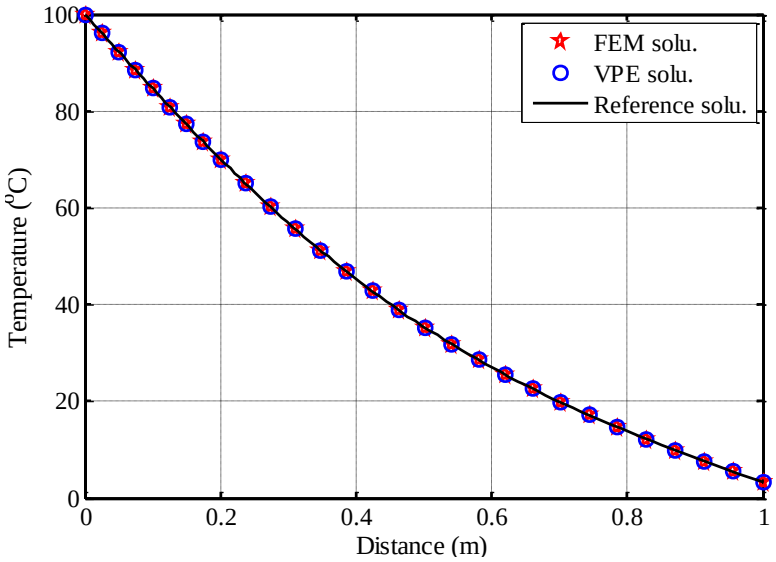

**Figure 8.**

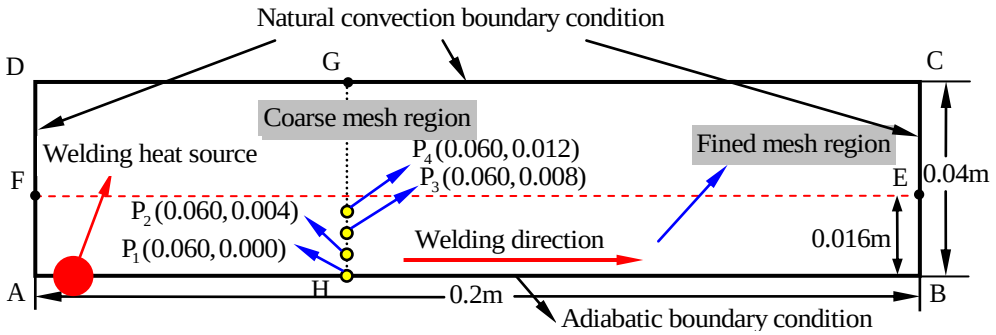


**Figure 9.**

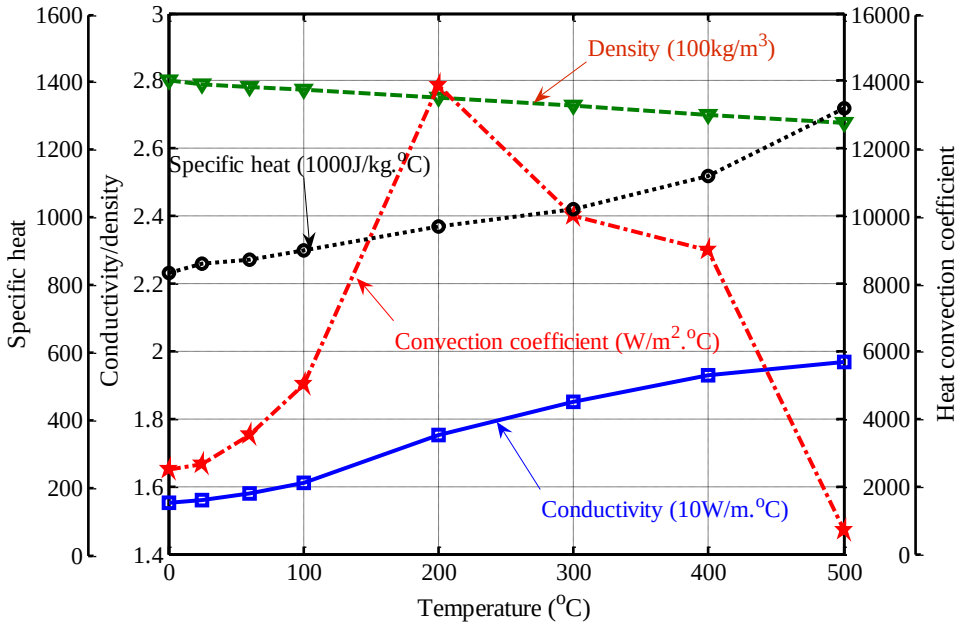


**Figure 10.**

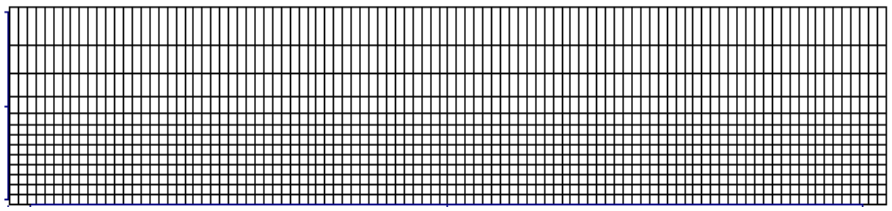

**Figure 11.**

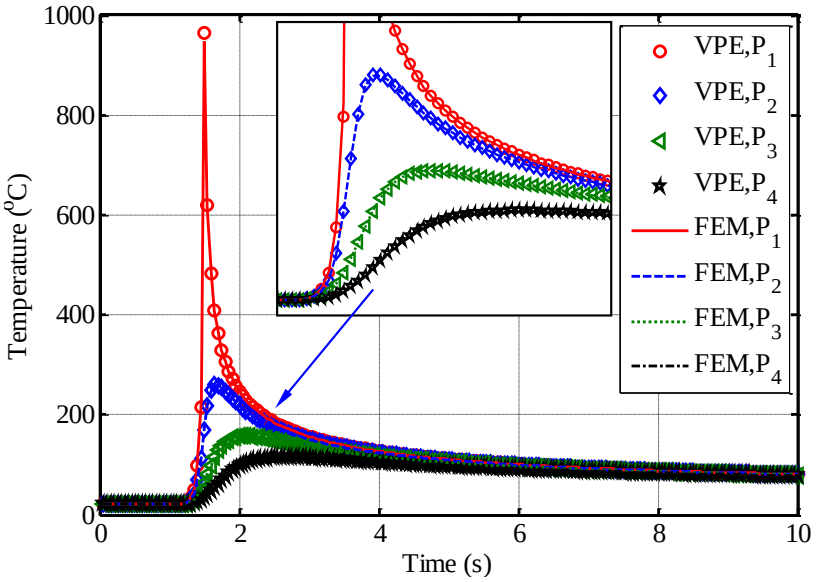


**Figure 12.**

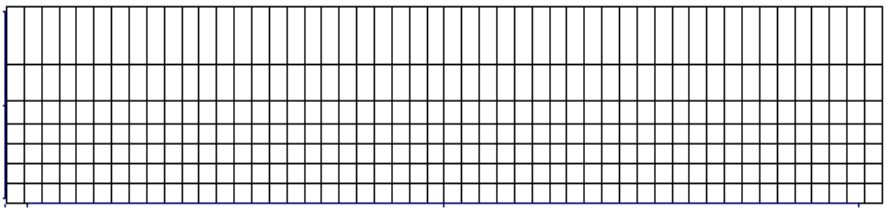

**Figure 13.**

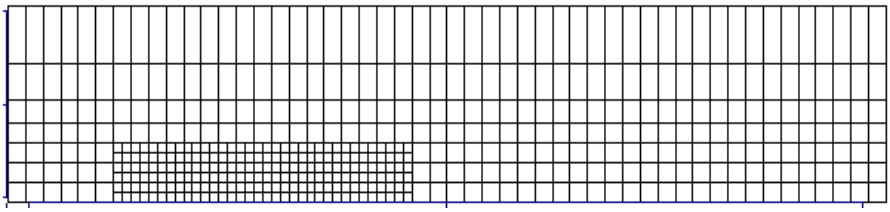

**Figure 14.**

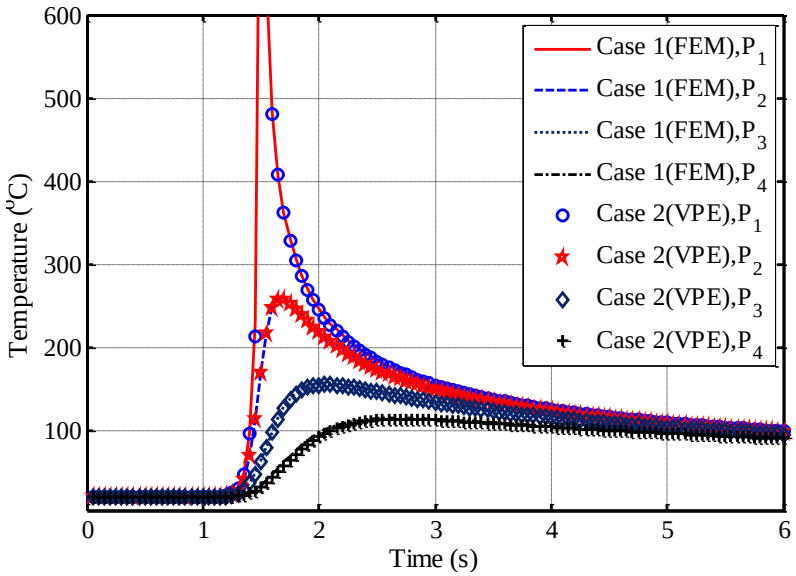


**Figure 15.**

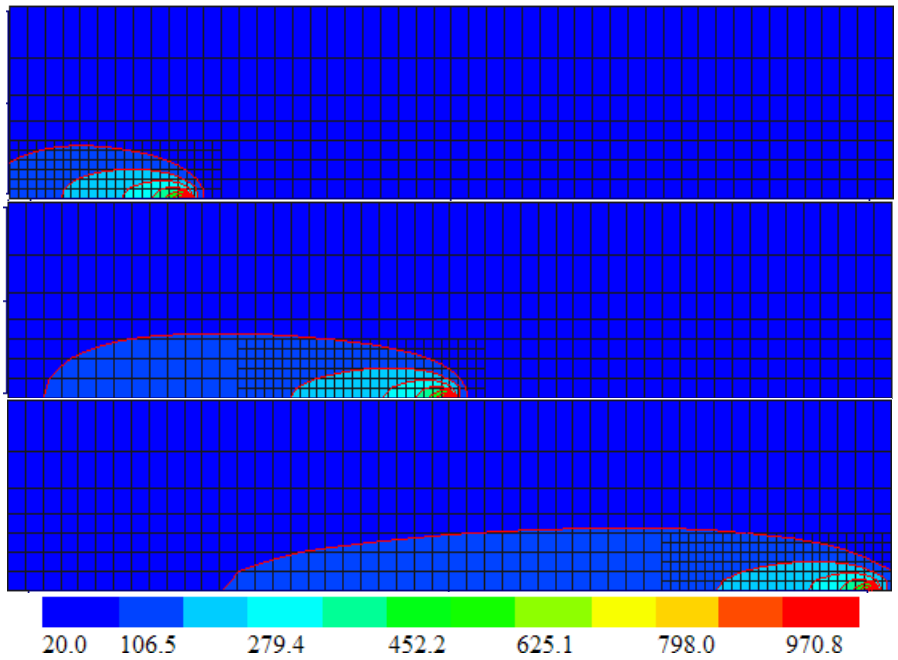

**Figure 16.**

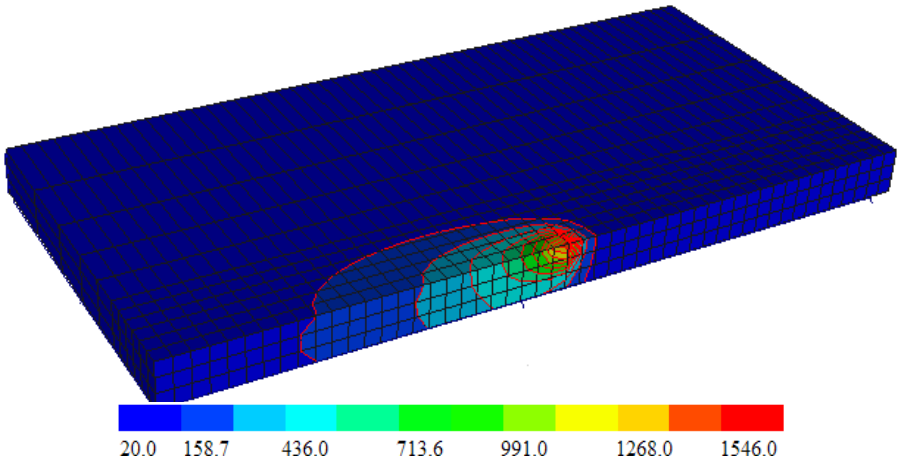


**Figure 17.**

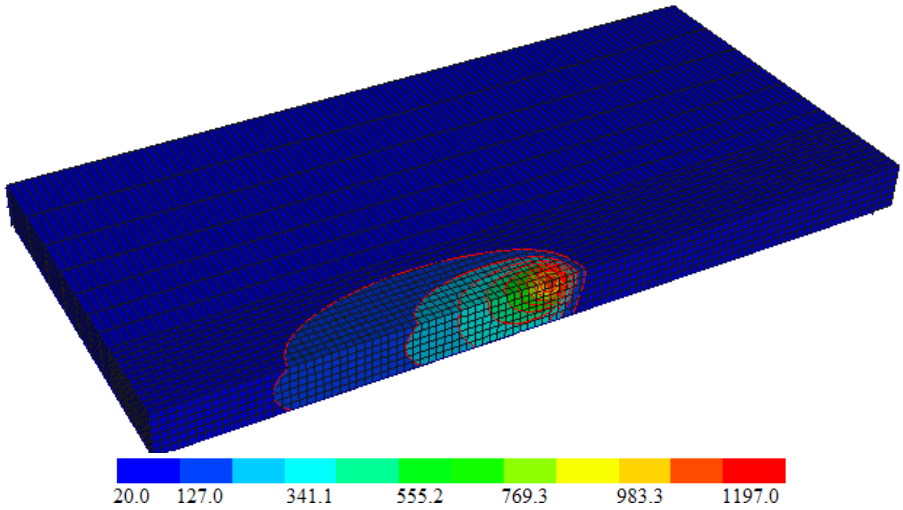

**Figure 18.**

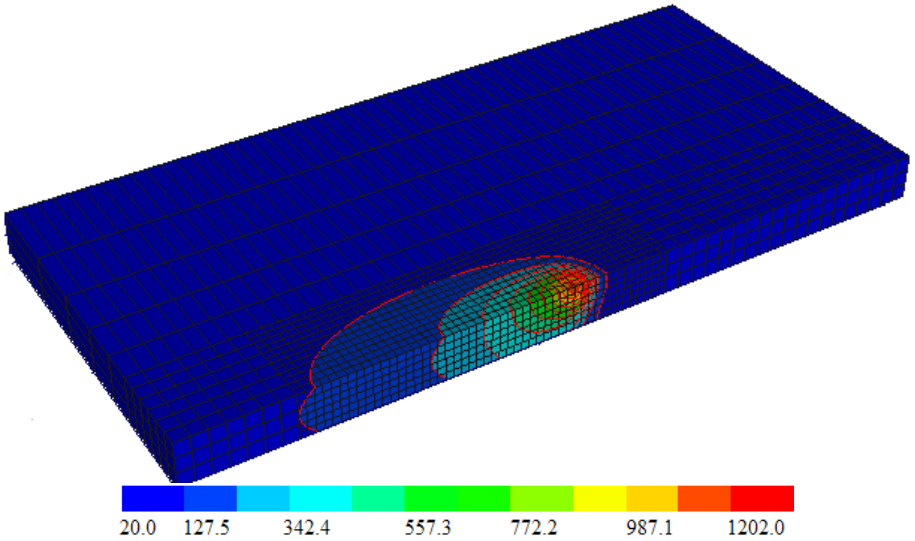


**Figure 19.**